Parametric Optimization for Thermoacoustic Refrigerator Driven by Thermoacoustic Engine

Ussama Ali[1], Md Islam[1], Isam Janajreh[1]
[1]Khalifa University of Science and Technology
Abu Dhabi, UAE
ussama.ali@ku.ac.ae; didarul.islam@ku.ac.ae; isam.janajreh@ku.ac.ae

Abstract - In this work, high fidelity numerical modelling is carried out to demonstrate the working of thermoacoustic refrigerator (TAR) coupled with thermoacoustic engine (TAE). The computational domain consists of two stacks, one for TAE and the other for TAR, in a long resonator tube which represent an actual physical model. The TAE stack's horizontal walls are imposed with a temperature profile with decreasing gradient, whereas convective heat transfer coefficient is applied to the thin vertical walls. The numerical model solves unsteady Navier-Stokes equations in non-isothermal flow. Numerical simulations are done on Ansys/fluent. Air is used as the working gas. Pressure, velocity, and temperature fields are computed and recorded at various locations in the domain. The TAR stack is considered fully coupled and is conjugated with the flow. For the development of pressure wave, working gas is considered as compressible with the density varying according to the ideal gas law. The effect of varying heating source temperature and varying the lengths of both the stacks is investigated on the output parameters, specifically the temperature drop at the cold end of the TAR stack, and pressure & velocity of the developed acoustic wave. The most favourable results in terms of temperature drop were obtained with 1:2 stack ratio and with heating temperature of 700K. It was observed that the acoustic wave with high amplitude of pressure and velocity does not necessarily produce maximum cooling.

Keywords: Heat to sound energy; Thermoacoustic refrigeration; CFD; High fidelity numerical modelling

1. Introduction

Acoustic wave can be generated by heating one end of the stack inside the resonator tube and cooling another end, as a result the gas inside the tube may spontaneously oscillate thereby giving rise to the acoustic wave [1]. Thermoacoustic devices operate on this phenomenon, producing acoustic wave using temperature gradient in Thermoacoustic Engine (TAE) or producing a cooling effect using the acoustic wave in Thermoacoustic Refrigerator (TAR) [2]. Thermoacoustic devices have attracted wide attention recently due to their high reliability and low maintenance cost as they have no moving parts and do not use harmful fluids as in the case for conventional engines or refrigerators [3, 4]. Thermoacoustic refrigerator can directly consume acoustic power produced by TAE to pump heat which produces cooling load. By combining TAE and TAR, low-grade thermal energy, such as solar energy, industrial waste heat, and geothermal energy can be utilized to produce the cooling effect. From the estimation by Lawrence Livermore National Laboratory, about 67.1% of the total energy consumption in 2020 in the United States was lost as waste heat [5].

Conventional refrigeration consumes a high-grade energy (electricity) and the refrigerants used are not environmentally friendly. Moreover, conventional cooling systems have many parts such as condenser, evaporator, compressor, and tubes etc., which increase their maintenance cost. For combined TAE-TAR device, renewable energy and low-grade energy, such as, concentrated solar power or various sources of waste heat can be utilized to generate acoustic wave to drive thermoacoustic refrigerator to get the desired temperature drop. This direct and tightly coupled integration is a complete green technology and environmentally safe. In TAR, there are no moving parts, and this gives them the advantage of being more reliable and low cost as they can operate without the need for exotic materials and precision machining or tight tolerances. Despite these advantages, the thermoacoustic devices are not extensively seen in practice and are still in developmental phase. One of the biggest challenges faced by the thermoacoustic devices is that they suffer from poor energy conversion efficiency, whether it is the conversion of thermal energy to acoustic energy in TAE or the opposite in TAR. Also, TARs suffer from low coefficient of performance (COP) which is usually about 1, compared to 2 to 6 for conventional

refrigerators. One of the reasons behind this poor performance is that the compression of gas in TAR takes more energy compared with vapor compression refrigerators [6].

The effectiveness of the thermoacoustic refrigeration system was examined in some works [7-10]. Panara et al. [7] found the significant factors affecting the TAR performance which include working gas, stack size and material properties, resonator shape, the stack arrangement, and the operating pressure. The key component in both TAE and TAR is the stack, which is a porous solid structure housed in between the two heat exchangers. Heat transfer takes place between the working fluid and the external heat source via the two heat exchangers placed at both ends of the stack. Results obtained in the work of the authors [7] indicated that the temperature variation of TAR was only 0.5°C along the resonator tube without the stack, and the presence of stack created an obvious temperature difference. In their work, 7°C temperature difference was observed in experiments. The performance of TAR in different operating conditions was studied by Nayak et al. [8] and they found that increasing heating load in the parallel plate stack help to obtain higher temperature drop. George [9], in his experimental study, found that increasing the length of the tube increased the temperature at the hot end of the TAR stack. He also concluded that TAR stack material with low thermal conductivity is more suited for the operation as it resists the heat diffusion between hot end and cold end of the stack. Hariharan et al. [10] studied the effect of stack plate thickness and spacing and found that thick stack plates resulted in higher, whereas stack with larger spacing between the plates resulted in lower temperature difference. The stack spacing is limited by parameters like thermal penetration depth (δ_k) and viscous penetration depth (δ_v). Successful operation of thermoacoustic devices require the spacing between the plates to be roughly a few times the thermal penetration depth [11].

The initial numerical studies of TAR involved simplifying the computational domain by considering a single stack without heat exchangers in a small domain. This was called as Thermoacoustic Couple (TAC) [12]. CFD is extensively applied for modelling thermoacoustic systems for evaluation of the performance, and to capture viscous and thermal losses. It can be used to identify the main parameters that affect the system performance and how to enhance their low efficiency. These parameters can be used to design and optimize the system, like stack porosity, stack location and its length, blockage ratio, working gas, and resonator tube length. Numerical modelling of TAR is expensive in terms of computational resources due to the fine mesh and small time-step requirements. However, with the advancements in the technology and with the increase in computational power, numerical models can be analysed with high fidelity. Energy and heat fluxes across the TAC of an isothermal short stack was computed by Cao et al. [13]. Later, Ishikawa and Mee [14] extended their work and examined the influence of spacing between the stack plates on the performance of the system. Two-dimensional computational fluid dynamics (CFD) has been used to successfully capture the velocity and temperature profiles inside parallel heat exchangers for a standing wave thermoacoustic system [15]. Ali et al. [16] carried out numerical analysis of TAR coupled with TAE and tested various working gases in the model. It was reported that the maximum temperature drop of 10.49°C was obtained with argon as the working gas.

Although the sporadic research is being conducted on thermoacoustic devices recently, still their full potential has not been unlocked, and more work needs to be done to bring this technology out of the laboratory and into the practical world. Only a few studies have been conducted incorporating a fully coupled thermoacoustic system. This work attempts to demonstrate the modelling of TAE and TAR as a coupled system. Here we investigate the effect of heating source temperature and the ratio of length of TAE stack to TAR stack on the performance of the system in terms of the acoustic wave and temperature drop at the cold end of TAR stack.

2. Methodology

The performance of thermoacoustic refrigerator operating on thermoacoustic engine is numerically tested in this work. Air is used as the working gas and the properties of air are shown in Table 1. The TAE stack is applied with constant temperature gradient with hot side temperature varied for each run and cold side fixed at 300K. The hot side temperature is varied between 500K and 1000K to study the effect of heating source temperature. In the thermoacoustic devices, the two parameters related to the working gas play a very important role, and they are the two characteristic

lengths: thermal penetration depth (δ_k) and viscous penetration depth (δ_v). These parameters determine how far heat and momentum can diffuse laterally, and are mathematically defined as:

$$\delta_\kappa = \sqrt{2\alpha/\omega}, \quad \text{where } \alpha = k/\rho c_p \tag{1}$$

$$\delta_v = \sqrt{2v/\omega}, \quad \text{where } v = \mu/\rho \tag{2}$$

where α is the thermal diffusivity, ρ is the density, k is the thermal conductivity of the working gas, c_p is the specific heat capacity, and μ and v are the dynamic and kinematic viscosities, respectively. Angular frequency (ω) is defined as $\omega = 2\pi f$, where f is the frequency of the acoustic wave. The viscous and thermal penetration depth for this analysis are 0.148 mm and 0.128 mm, respectively, for air as the working fluid.

Table 1: Properties of the working fluid (Air)

Property	Value
Density, ρ (kg/m^3)	1.225
Specific heat capacity, c_p (J/kgK)	1006.43
Thermal conductivity, k (W/mK)	0.0242
Dynamic viscosity, μ (kg/ms)	1.79×10^{-5}
Viscous penetration depth, δ_v (mm)	0.148
Thermal penetration depth, δ_k (mm)	0.128

2.1. Computational Domain

The computational domain consists of a long circular tube with length to diameter ratio (L/D) of 10 housing two circular stacks. One half plane of the tube is considered for the computational domain taking advantage of the axisymmetric of the physical system. TAE and TAR stacks are centred at 0.1L and 0.3L from the closed end of the tube, respectively, where L is the length of the tube. Placing the TAR stack near the open end of the tube would require very fine mesh throughout the domain for the pressure wave to travel through, which would increase the computational time considerably, therefore TAR stack is also placed near the closed end at a distance of 0.3L. The length of each stack is 1 cm. For both the stacks, the thickness of each stack plate and the spacing between the plates is taken as 0.5 mm, this constitutes 3.9 times the thermal penetration depth. This value gives the required imperfect contact of the working gas with the stack walls, a condition necessary for the proper operation of the thermoacoustic system.

Figure 1 shows the schematics of the computational domain, the figure is not to scale (inflated in the vertical direction), and it only emphasizes the heat exchangers and the stacks. Figure 2 shows the complete computational domain along with the zoomed in view of the stacks. Fine meshing can be seen near the stack walls. The setup for the standing wave has one closed- and one open-end which results in quarter wavelength of the pressure wave inside the domain, i.e., the wavelength (λ) of the wave generated is 4L.
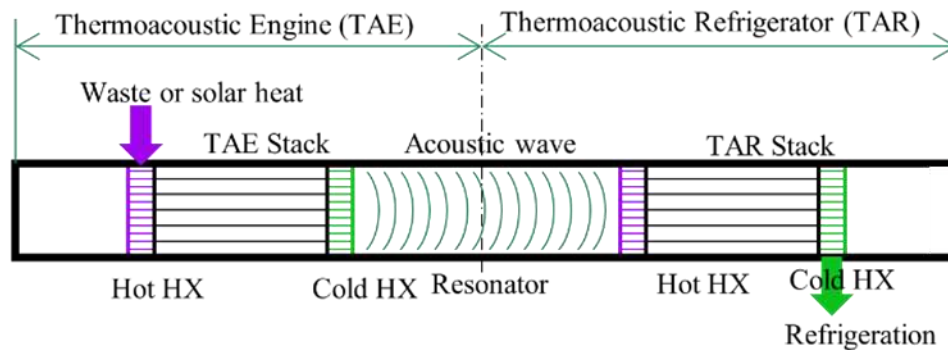
Fig. 1: Resonator tube containing TAE and TAR stacks

The high temperature standing wave TAE in this setup uses a high heat source of 500K – 1000K at the inlet temperature of the hot heat exchanger to simulate flue gasses from a burner, solar sources, or even a steel furnace smelter. Thermoacoustic heat pumping device feeds on the prime mover's acoustical signal and pumps heat. The stack material is taken as a combination of fiberglass and stainless steel as used by Abd El-Rahman and coworker [17]. The effective density, specific heat capacity, and thermal conductivity of the stack material is 5082 kg/m^3, 683.5 J/kg.K and 5.76 W/mK, respectively. The stack material with low thermal conductivity is preferable as it will restrict the heat transfer between the cold and hot end of the TAR.
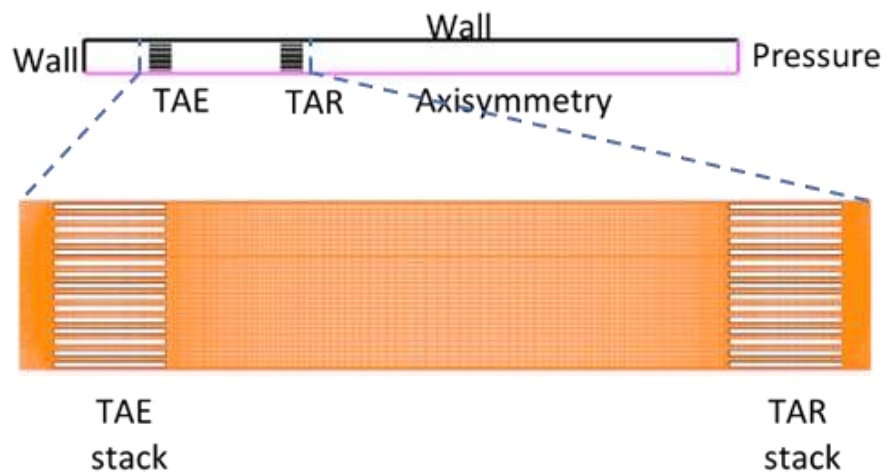
Fig. 2: Computational domain along with zoomed in view of the section containing TAE and TAR stacks

2.3. Governing Equations

Numerical modelling of the setup is based on the transient, non-isothermal Navier-Stokes flow equations which represents the conservative laws (mass, momentum, and energy). The ideal gas model is assumed that governs the gaseous fluid state and turbulence is accounted for by averaging the governing equations leading to Reynolds stresses which are modelled via the common eddy viscosity and k-ε transport model. Equations 3 to 9 describe the overall governing equations. Eq. 3 is the continuity, Eqs. 4, 5, and 6 are the momentum, and Eq. 8 is the general transport equation for any of the scalar quantity. In this analysis this equation is used for defining turbulent kinetic energy (k) and its rate of dissipation (ε), as k-ε turbulence model is used. Eq. 9 governs the energy equation.

The continuity equation for axisymmetric geometries is given as below:

$$\frac{\partial \rho}{\partial t} + \frac{\partial (\rho V_x)}{\partial x} + \frac{\partial (\rho V_r)}{\partial r} + \frac{\rho V_r}{r} = 0 \tag{3}$$

where x and r are the axial and radial coordinates, respectively, and V_x and V_r are the axial and radial velocity, respectively.

The momentum equation is given as:

$$\frac{\partial (\rho \vec{V})}{\partial t} + \nabla.(\rho \vec{V} \vec{V}) = -\nabla p + \nabla.\mu[(\nabla \vec{V} + \nabla \vec{V}^T) - \frac{2}{3} \nabla.\vec{V}I] + \rho \vec{g} \tag{4}$$

where p is the static pressure, μ is the molecular viscosity, and I is the unit tensor and its term accounts to the effect of volume dilation/expansion. The ρg term is the gravitational body forces vector.

The momentum equations for 2D axisymmetric geometries in the axial and radial direction are given as:

$$\frac{\partial \rho V_x}{\partial t} + \frac{1}{r}\frac{\partial}{\partial x}(r\rho V_x V_x) + \frac{1}{r}\frac{\partial}{\partial r}(r\rho V_r V_x) = -\frac{\partial p}{\partial x} + \frac{1}{r}\frac{\partial}{\partial x}[r\mu(2\frac{\partial V_x}{\partial x} - \frac{2}{3}(\nabla.\vec{V}))] + \frac{1}{r}\frac{\partial}{\partial r}[r\mu(\frac{\partial V_x}{\partial r} - \frac{\partial V_r}{\partial x})] + \rho g_x \tag{5}$$

$$\frac{\partial \rho V_r}{\partial t} + \frac{1}{r}\frac{\partial}{\partial x}(r\rho V_x V_r) + \frac{1}{r}\frac{\partial}{\partial r}(r\rho V_r V_r) = -\frac{\partial p}{\partial r} + \frac{1}{r}\frac{\partial}{\partial x}[r\mu(\frac{\partial V_r}{\partial x} + \frac{\partial V_x}{\partial r})] + \frac{1}{r}\frac{\partial}{\partial r}[r\mu(2\frac{\partial V_r}{\partial r} - \frac{2}{3}(\nabla.\vec{V}))] - 2\mu\frac{V_r}{r^2} + \frac{2\mu}{3r}(\nabla.\vec{V}) + \rho g_r \tag{6}$$

Divergence in axisymmetric geometries is as:

$$\nabla.\vec{V} = \frac{\partial V_x}{\partial x} + \frac{\partial V_r}{\partial r} + \frac{V_r}{r} \tag{7}$$

The transport equation in terms of ϕ for each of the two turbulence scalars is given as:

$$\frac{\partial (\rho \phi)}{\partial t} + \nabla.(\rho \vec{V} \phi - \Gamma \nabla \phi) = S_{\phi_k} \tag{8}$$

where ϕ is a scaler quantity representing k and ε. S is the source term and Γ represents the diffusion coefficient.

The internal energy (E) equation is given as:

$$\frac{\partial (\rho E)}{\partial t} + \nabla.(\rho \vec{V}(\rho E + p)) = -\nabla.[K\nabla T + (\mu(\nabla \vec{V} + \nabla \vec{V}^T) - \frac{2}{3}\nabla.\vec{V}I).\vec{V}] \tag{9}$$

where p is the pressure, ρ and μ represent the fluid density and viscosity, respectively, μ_T is the turbulent viscosity, and $\vec{V}$ represents the velocity field. The internal energy (E) of the system is given by the equation below:

$$E = H - p/\rho + 0.5\vec{V}.\vec{V} \tag{10}$$

where H is the system enthalpy. The numerical solution is sought for the Equations 3-10 by discretizing the flow domain and using the finite volume method. The first-order fully implicit scheme is used for discretization in time and the second-order central difference scheme is used space.

With respect to boundary conditions, as shown in Figure 2, all walls except the outlet are prescribed no slip. The bottom wall is assigned as symmetry. A free pressure outflow is set at the outlet. For the horizontal walls of the TAE stack a decreasing temperature gradient profile is applied from 700K to 300K. The vertical walls of the stack are prescribed a 50 W/m²K heat transfer coefficient. The k-ε turbulence model is used with standard wall function to account for the turbulence. Transient analysis is carried out with a time step of 1×10^{-5} sec, in accordance with the Courant-Friedrichs-Lewy number (CFL) principal.

3. Results and Discussion

Owing to the extremely small timestep of 1×10^{-5} sec, the model is run for 1.5 seconds of flow time which required 150,000 timesteps with each timestep comprising 40 iterations. The convergence criterion for the solution is set as 1×10^{-8}. The results are recorded when the flow was fully developed, and the pressure wave became completely periodic. The time span of 1 second for each run is very small considering the physical application of the model, but it was sufficient for the

simulation as the flow became pure periodic. Pressure and axial velocity are measured at the point midway between the TAE and TAR stacks. Using the periodic wave data, Fast Fourier Transform (FFT) is done to obtain the frequency of oscillations.

Figure 3 shows the variation in pressure and velocity for the developed acoustic wave and its frequency spectrum obtained using FFT. The results in this figure are for the configuration with TAE : TAR stack length of 1:1, and with the hot end temperature of TAE stack of 1000K. The pressure and axial velocity propagation in time is shown for 0.02 seconds of flow time. It can be observed that the phase angle between the pressure and velocity is close to 90 degrees, thereby confirming it as a standing wave. The obtained frequency of 305Hz is slightly different from the theoretical value of 286 Hz. One possible reason is that for theoretical calculation using the formula $f = c/\lambda$, the speed of sound (c) is taken as a fixed value at 300K whereas in the recorded data, the local changes in the gas properties affect this value which in turns affects the measured frequency of the acoustic wave.
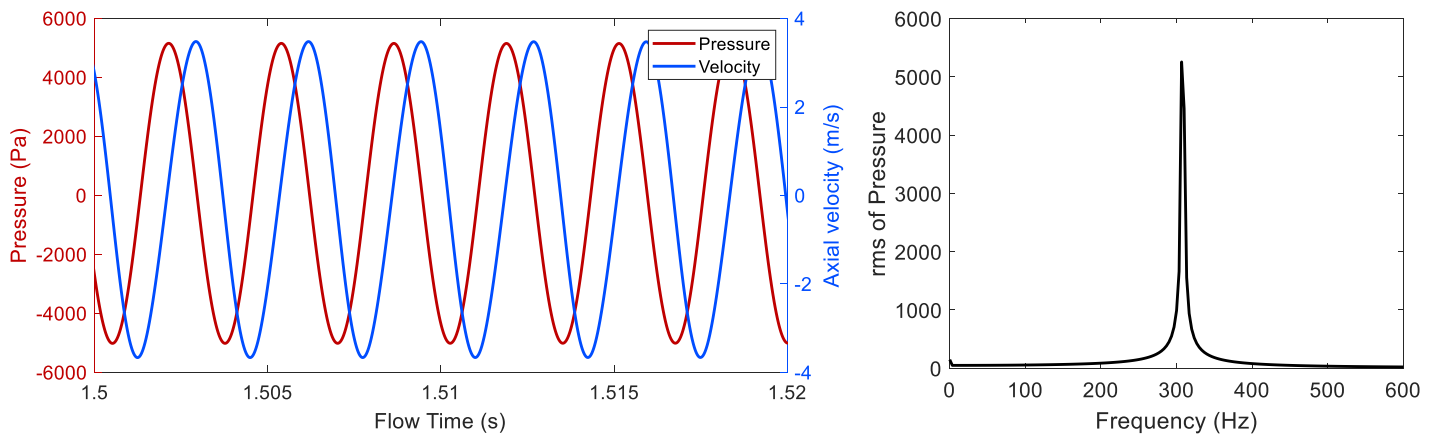
Fig. 3: The developed pressure and velocity wave (left), and the frequency spectrum for the acoustic wave (right)

Table 2 represents the data for all the cases considered in this study. The configuration of the computational model is given in terms of the ratio of TAE stack length to TAR stack length. This is the one variable in this study along with the temperature of the hot end of the TAE stack. The results are presented in terms of amplitude of pressure and axial velocity and their rms values. The cold end temperature of the TAR stack is also given along with the temperature drop between the two ends of TAR stack. It must be noted that cold end of TAE stack and hot end of TAR stack both are fixed at 300K. These results are depicted in Figure 4. It is observed that increasing the heat source temperature increases both the pressure and velocity of the developed acoustic wave, however the maximum temperature drop is observed at 700K heat source temperature. Changing the ratio of the lengths of TAE and TAR stack, the maximum temperature drop of 7.13 °C is observed with 1:2 configuration, which means the length of TAR stack is twice that of the length of TAE stack. The pressure and velocity amplitude observed is lowest of the three cases but results in higher temperature drop.

Table 2: The temperature drop obtained with different configurations

TAE stack length : TAR stack length	Hot end temperature of the TAE stack	Pressure amplitude	Rms of pressure	Axial velocity amplitude	Rms of axial velocity	Cold end temperature of the TAR stack	Temperature drop
(-)	(K)	(Pa)	(Pa)	(m/s)	(m/s)	(K)	(°C)
1 : 1	500	166.23	114.75	0.1316	0.0891	299.45	0.55
1 : 1	700	3712.8	2593.6	2.7700	1.9200	294.06	6.02
1 : 2	700	1846.8	1286.4	1.3609	0.9263	292.87	7.13
2 : 1	700	2696.1	1881.8	1.8591	1.3022	293.86	6.14
1 : 1	1000	5152.5	3599.7	3.5491	2.4982	294.13	5.87
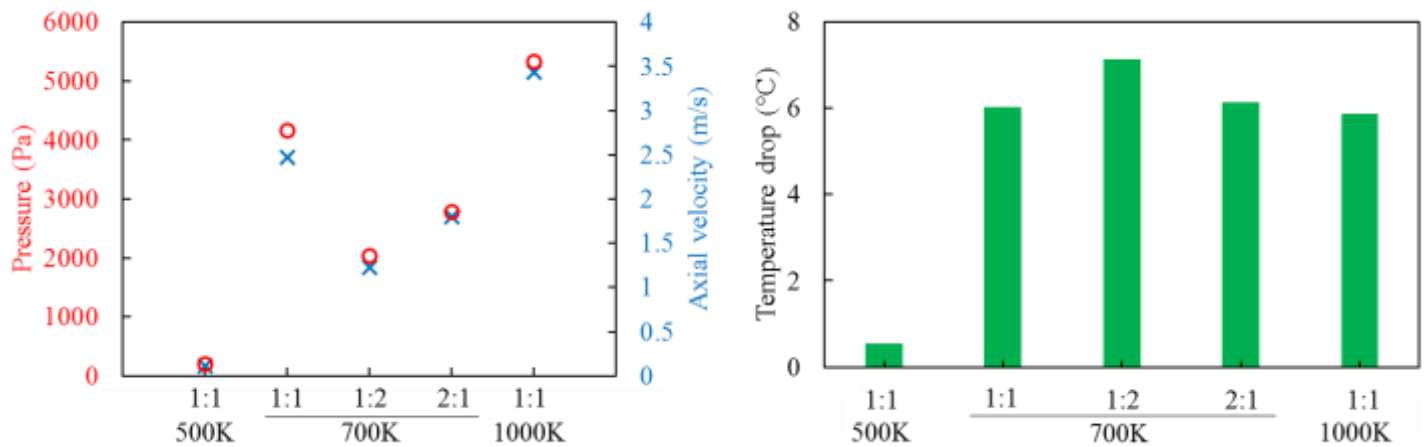
Fig. 4: Amplitude of pressure and axial velocity (left), and the temperature drop observed at the cold end temperature of TAR stack (right)

4. Conclusion

Numerical simulation of thermoacoustic refrigerator, operating on the acoustic wave generated by thermoacoustic engine, is carried out in this study. The computational domain closed at one end and open at the other resulted in the generation of standing wave. Three levels of heating were considered, and three levels of the configurations were considered in terms of the ratio of TAE stack length to TAR stack length. The maximum temperature drop of 7.13 °C was observed in the case of 1:2 configuration with heating source temperature of 700K. However, the maximum amplitude of acoustic pressure and axial velocity was observed with the heating temperature of 1000K. Therefore, it is not necessary that acoustic wave with highest energy will always produce maximum cooling.

References

[1] J. Wheatley, T. Hofler, G. W. Swift, and A. Migliori, "Understanding some simple phenomena in thermoacoustics with applications to acoustical heat engines," *American Journal of Physics*, vol. 53, no. 2, pp. 147–162, Feb. 1985, doi: 10.1119/1.14100.

[2] A. Tominaga, "Thermodynamic aspects of thermoacoustic theory," *Cryogenics*, vol. 35, no. 7, pp. 427–440, Jul. 1995, doi: 10.1016/0011-2275(95)93576-L.

[3] G. W. Swift and S. L. Garrett, "*Thermoacoustics: A Unifying Perspective for Some Engines and Refrigerators*," *The Journal of the Acoustical Society of America*, vol. 113, no. 5, pp. 2379–2381, May 2003, doi: 10.1121/1.1561492.

[4] T. Jin, J. Huang, Y. Feng, R. Yang, K. Tang, and R. Radebaugh, "Thermoacoustic prime movers and refrigerators: Thermally powered engines without moving components," *Energy*, vol. 93, pp. 828–853, Dec. 2015, doi: 10.1016/j.energy.2015.09.005.

[5] Lawrence Livermore National Laboratory, Estimated U.S. energy consumption in 2020. https://flowcharts.llnl.gov/content/assets/images/charts/Energy/Energy_2020_United-States.png (accessed Mar. 13, 2022).

[6] C. Herman and Z. Travnicek, "Cool sound: the future of refrigeration? Thermodynamic and heat transfer issues in thermoacoustic refrigeration," *Heat Mass Transfer*, vol. 42, no. 6, pp. 492–500,2006, doi: 10.1007/s00231-005-0046-x.

[7] K. S. Panara and A. M. Patel, "Thermoacoustic Refrigeration System Setup", *International Journal of Mechanical Engineering and Technology (IJMET)*, vol. 6, pp. 01-15, 2015.

[8] Ramesh Nayak. B, Bheemsha, Pundarika. G, Performance Evaluation of Thermoacoustic Refrigerator Using Air as Working Medium, *SSRG International Journal of Thermal Engineering (SSRG-IJTE)*, vol. 1, no. 2, Aug. 2015, doi: 10.14445/23950250/IJTE-V1I3P101.

[9] J. George, "Loud Speaker Driven Thermo Acoustic Refrigeration", *International Journal of Scientific &Engineering Research*, vol. 7, pp. 465-468, 2016.

[10] N. M. Hariharan, P. Sivashanmugam, and S. Kasthurirengan, "Experimental investigation of a thermoacoustic refrigerator driven by a standing wave twin thermoacoustic prime mover," *International Journal of Refrigeration*, vol. 36, no. 8, pp. 2420–2425, Dec. 2013, doi: 10.1016/j.ijrefrig.2013.04.017.

[11] G. W. Swift, "Thermoacoustic engines", *The Journal of the Acoustical Society of America*, vol. 84, 1988, pp. 1145–1180.

[12] J. Wheatley, T. Hofler, G. W. Swift, and A. Migliori, "An intrinsically irreversible thermoacoustic heat engine," *The Journal of the Acoustical Society of America*, vol. 74, no. 1, pp. 153–170, Jul. 1983, doi: 10.1121/1.389624.

[13] N. Cao, J. R. Olson, G. W. Swift, and S. Chen, "Energy flux density in a thermoacoustic couple," *The Journal of the Acoustical Society of America*, vol. 99, no. 6, pp. 3456–3464, Jun. 1996, doi: 10.1121/1.414992.

[14] H. Ishikawa and D. J. Mee, "Numerical investigations of flow and energy fields near a thermoacoustic couple," *The Journal of the Acoustical Society of America*, vol. 111, no. 2, pp. 831–839, Feb. 2002, doi: 10.1121/1.1430687.

[15] F. Mohd Saat and A. Jaworski, "The Effect of Temperature Field on Low Amplitude Oscillatory Flow within a Parallel-Plate Heat Exchanger in a Standing Wave Thermoacoustic System," *Applied Sciences*, vol. 7, no. 4, p. 417, Apr. 2017, doi: 10.3390/app7040417.

[16] U. Ali, I. Janajreh, M. Islam and S. Abedrabbo, "Numerical Simulation Of Thermoacoustic Refrigerator Coupled With Thermoacoustic Engine", *15th International Conference On Heat Transfer, Fluid Mechanics And Thermodynamics Proceedings (HEFAT 2021)*, Pg. 1666-1671.

[17] A. Abd El-Rahman and E. Abdel-Rahman, "Numerical simulation of a thermoacoustic couple," in *Acoustics 2012*, Nantes, France, Apr. 2012. Accessed: Mar. 13, 2022. [Online]. Available: https://hal.archives-ouvertes.fr/hal-00810707